Design of a Stacked Co-Polarized Full-Duplex Antenna With Broadside Radiation

Weiquan Zhang, Jiadong Hu, Yue Li, *Senior Member, IEEE*, and Zhijun Zhang, *Fellow, IEEE*

***Abstract*— This article presents a co-linearly polarized (LP) stacked two-port antenna with compact size and broadside radiation patterns for in-band full-duplex (IBFD) application. The proposed IBFD antenna consists of a patch antenna and a substrate integrated waveguide (SIW) cavity-backed slot antenna (CBSA). The patch antenna and the CBSA are used as the transmitter (Tx) and receiver (Rx), respectively. The Rx is placed above the Tx for compact size. Linear polarization and broadside radiation patterns are achieved in this article. A cavity-patch coupling (CPC) path is added for canceling the slot-patch coupling (SPC) by using four probes to connect the top layer of the SIW cavity and the metal ground. Parametric studies show that the two coupling paths can be adjusted independently. Experimental results illustrate that the measured highest isolation over 40 dB is obtained with a compact size of $30 \times 30 \times 4$ mm^3 ($0.63\lambda_0 \times 0.63\lambda_0 \times 0.08\lambda_0$, λ_0 is the free-space wavelength at the center frequency of about 6.29 GHz). The measured −10 dB bandwidths of the Tx and Rx antennas are 430 and 100 MHz, respectively. The proposed stacked IBFD antenna is validated with the merits of identical polarization, same radiation direction, and compact size.**

***Index Terms*— Broadside radiation, duplexers, mutual coupling (MC), patch antenna, substrate integrated waveguide (SIW) cavity-backed slot antenna (CBSA).**

I. Introduction

IN-BAND full-duplex (IBFD) transceivers have gained great attention for alleviating the limited available bandwidth challenge with the ever-increasing demand for wireless communication. Compared with time-division duplex and frequency-division duplex, the IBFD is able to transmit and receive data over the same frequency band simultaneously. Hence, the spectral efficiency of wireless communication systems can be doubled by applying the IBFD technique [1]. It is a challenge to reduce the self-interference between the transmitter (Tx) and the receiver (Rx) channels for high interport isolation. The demanded level for SI cancellation depends on the level of the transmitted signal. The techniques to decrease the SI can be divided into three domains: analog, digital, and antenna cancellation [2]–[6].

Manuscript received September 13, 2020; revised March 23, 2021; accepted April 10, 2021. Date of publication May 5, 2021; date of current version October 28, 2021. This work was supported in part by the National Natural Science Foundation of China under Contract 61971254 and Contract 61525104, and in part by the National Key Research and Development Program of China under Grant 2018YFB1801603. *(Corresponding author: Zhijun Zhang.)*

The authors are with the Department of Electronic Engineering, Tsinghua University, Beijing 100084, China, and also with the Beijing National Research Center for Information Science and Technology, Tsinghua University, Beijing 100084, China (e-mail: zjzh@tsinghua.edu.cn).

Color versions of one or more figures in this article are available at https://doi.org/10.1109/TAP.2021.3076587.

Digital Object Identifier 10.1109/TAP.2021.3076587

In the antenna domain, there are many antenna techniques for achieving high interport isolation. The interport isolation is basically based on polarization diversity [7]–[14], antenna separation [15], spatial phase diversity [16]–[20], neutralization line [21], parasitic structure [22]–[25], metamaterial [26], and placement of absorbers between antennas [27], [28]. Co-circularly polarized IBFD antennas were proposed in [17] and [19] with four concentrically arranged radiating elements. Beamforming networks were used in these works for achieving circular polarization. These feeding networks increased the size of the antennas to a certain extent. In fact, there are many other communication systems with linear polarization and limited space in practical applications. Hence, linearly polarized (LP) IBFD antennas without using any complicated feeding networks have the potential to be applied in space-limited LP communication systems. In [18], a wideband omnidirectional Tx antenna was placed at the field null of a symmetric Rx circular array. Therefore, 40 dB interport isolation with colinear polarization was achieved at the expense of high complexity and large antenna size. Also, the profile was too high to be planarly integrated. A signal path was established by adding a passive suspended neutralization line to increase the isolation between the two antennas in [21]. The two antennas were designed to operate at different frequencies, and extra space was required for the neutralization line. In [23], a parasitic structure was proposed for mitigating the mutual coupling (MC) between the two collinear dipoles while preserving omnidirectional radiation patterns. The complexity and size of the system were increased due to the introduction of the parasitic structure. Similarly, additional space is unavoidable for other decoupling structures, such as metamaterials and absorbers. Therefore, achieving an IBFD system with compact size and colinear polarization is still a challenge.

On the other hand, the MC of stacked antennas has received little attention. Only few references studying the MC between stacked patches can be found [29]–[32]; a 180° phase difference between the induced currents at the parasitic and driven patches was utilized for coupling reduction [32]. Two driven patches were separated in the azimuth plane, and the profile was relatively high due to the stacked parasitic patches. Thus, the design of a stacked co-polarized IBFD antenna with a low profile has yet to be reported in the open literature.

An IBFD system can be categorized as a monostatic system where a single aperture is used for Tx and Rx operations or a bistatic system in which separated Tx and Rx antenna apertures are utilized. Bistatic systems are usually

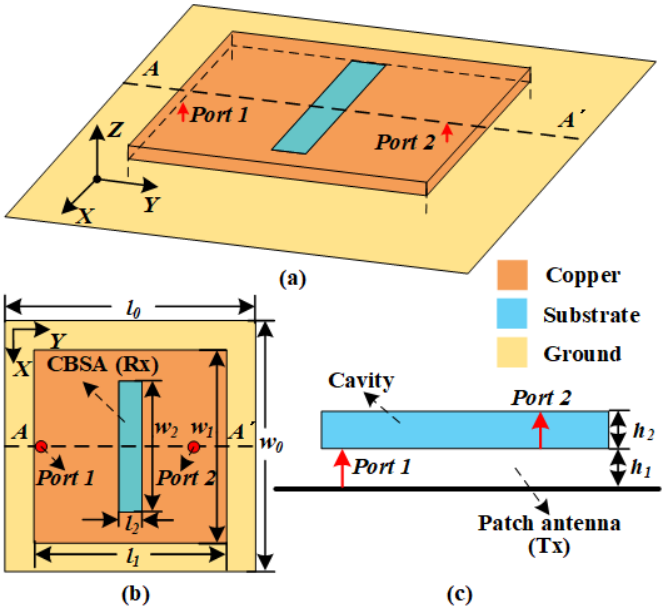

Fig. 1. Geometry of the proposed IBFD antenna. (a) 3-D view. (b) Top view (central plane AA'). (c) Side view.

bulky in geometry and unsuitable for space-critical applications. A bistatic configuration with high isolation can be implemented with an increase in the size [19], [23], [24]. To address this issue, the bottom layer of the cavity-backed slot antenna (CBSA) is reused as a patch antenna for compact size and a low profile in this article. Strong MC between the Tx and Rx antennas is inevitable due to the slot-patch coupling (SPC). A cavity-patch coupling (CPC) path is added by introducing four probes between the substrate integrated waveguide (SIW) cavity and the patch. Since the Tx and Rx antennas work at different modes, the four probes have dissimilar influences on them. Reduction of MC can be achieved by tuning the two coupling paths independently to cancel each other out. A prototype was fabricated to provide an experimental verification of the design.

This article is organized as follows. In Section II, the basic structure is presented and the MC between the Tx and Rx antennas is discussed. The decoupling mechanism and design guidelines of the proposed antenna are given in Section III. In Section IV, the antenna fabrication, simulated, and measured performances of the proposed antenna are indicated. Finally, conclusions are given in Section V.

II. Antenna Design

Fig. 1 shows the sketch diagram of the proposed IBFD antenna, which contains a rectangular patch antenna and a rectangular cavity. A slot is etched on the cavity, by which it can be excited. The CBSA functions as the Rx antenna and is placed above the patch antenna, which works as the Tx antenna. As shown in Fig. 1, the proposed antenna exhibits even-symmetrical property along the *XZ* plane and the *YZ* plane. Therefore, compact size is achieved. The detailed dimensions are given in Table I.

TABLE I
Detailed Dimension of the Proposed Antenna

Parameter	Value(mm)	Parameter	Value(mm)
l_0	40	w_0	40
l_1	26	w_1	26
l_2	2	w_2	16.5
h_1	2	h_2	2

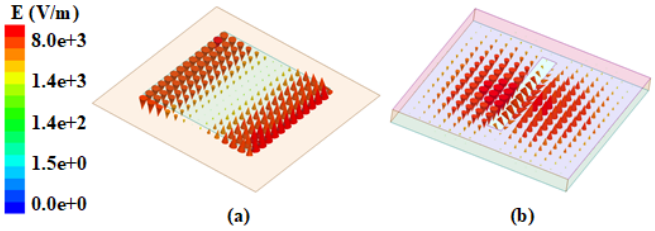

Fig. 2. Schematics of electric field distributions. (a) TM_{01} mode. (b) TE_{110} mode.

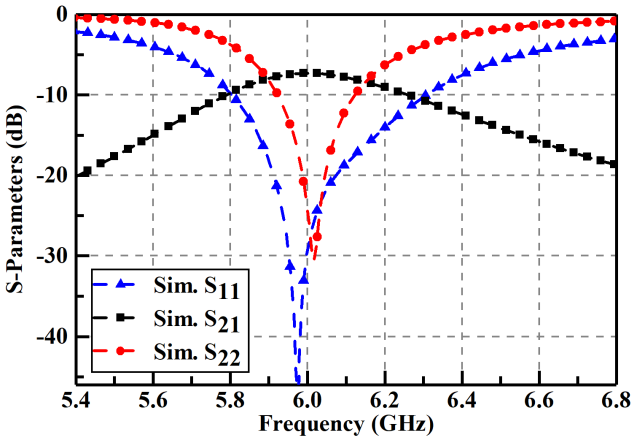

Fig. 3. Simulated S-parameters of the proposed antennas.

The TM_{01} mode of the patch antenna and the TE_{110} mode of the CBSA are excited here for effective radiation. It is known that the electrical field distribution beneath the patch antenna operating under TM_{01} mode is sinusoidal and odd-symmetric in the E-plane, whereas the electric field intensity is almost uniform in the H-plane. However, the electrical field distribution of the TE_{110} mode is sinusoidal in both the E-plane and the H-plane, as shown in Fig. 2. Hence, the operating frequencies of the patch antenna and the cavity can be tuned independently since they operate at different modes. The resonant frequency of the patch antenna is mainly determined by parameter l_1, whereas the resonant frequency of the CBSA can be adjusted by changing parameters l_1, w_1, and w_2. Besides, the filled substrate within the CBSA can also be employed to adjust the operating frequency of the CBSA. Therefore, it is achievable to adjust the resonant frequency of the CBSA with little influence on that of the patch antenna.

Fig. 3 shows the simulated S-parameters of the IBFD antenna. When the resonant frequencies of the Tx and Rx

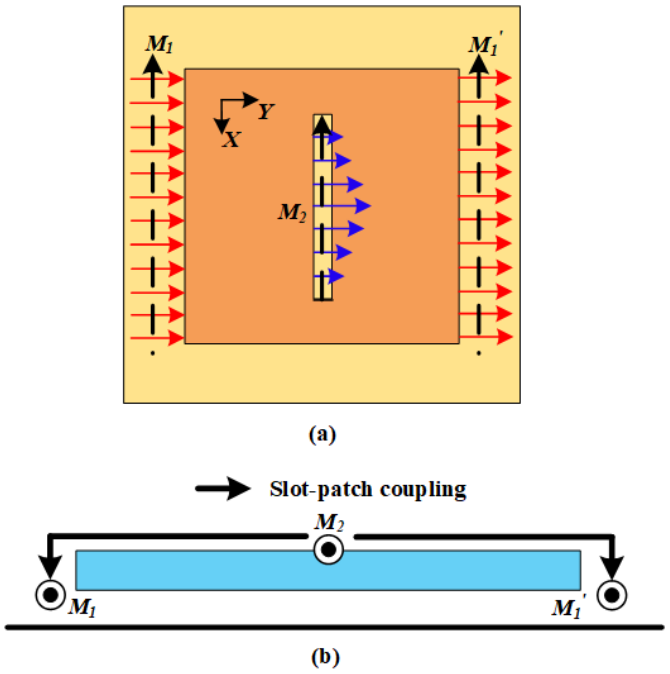

Fig. 4. Schematics of the Tx and Rx antennas to explain the radiation and coupling mechanism. (a) Equivalent magnetic currents. (b) SPC coupling path.

antennas are tuned to be almost identical, the isolation is only about 7 dB. It is noted that probes are used here to tune the resonant frequency of the Tx antenna but without deteriorating the TM_{01} mode. It is a challenge to mitigate the MC between the Tx and Rx antennas due to the initial high coupling level.

III. Antenna Analysis

To further uncover the decoupling principle, the proposed Tx and Rx antennas are investigated by their radiation mechanism and coupling paths. Then, a decoupling method is proposed and analyzed by parametric studies. Based on the analysis of the MC between the Tx and Rx antennas, design guidelines are finally given.

A. Radiation Mechanism and MC

To clearly explain the coupling principle of the proposed stacked IBFD antenna, Fig. 4(a) shows the equivalent magnetic currents of both the Tx and Rx antennas. Two corresponding equivalent magnetic currents (M_1 and M_1') of the patch antenna are obtained. Also, only one equivalent magnetic current (M_2) of the Rx antenna is acquired. The two magnetic currents (M_1 and M_2 or M_1' and M_2) are separated at a distance of about a quarter wavelength. Hence, the reduction of the MC between the Tx and Rx antennas is workable since their radiation apertures are separated in space. The coupling path of the SPC is shown in Fig. 4(b). It can be seen that the strong MC is caused by the electric fields, which propagates along the metal surface of the cavity from one port to the other port. Therefore, it is a key challenge to eliminate the MC between the slot and patch antennas without using complicated structures and deteriorating their radiation patterns.

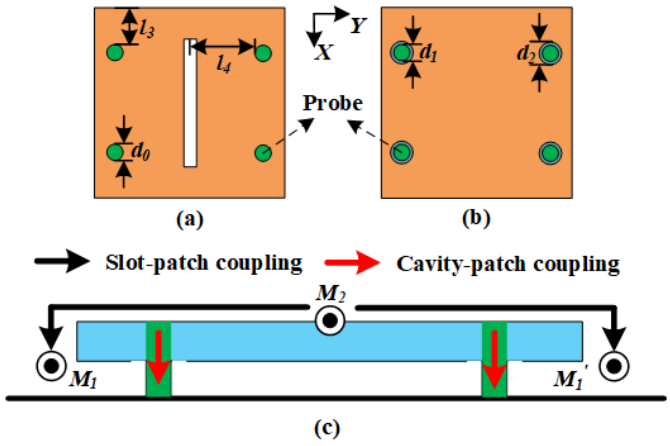

Fig. 5. Schematics of the decoupling mechanism. The four probes in (a) top and (b) bottom views of the CBSA. (c) Two coupling paths. $l_3 = 4.45$ mm, $l_4 = 10.75$ mm, $d_0 = 0.7$ mm, $d_1 = 1$ mm, and $d_2 = 1.4$ mm.

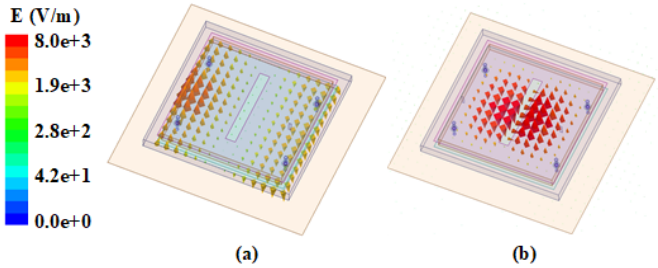

Fig. 6. Electric field distributions of the patch antenna and the CBSA with the four probes added. (a) Patch antenna. (b) CBSA.

B. Decoupling Mechanism

To increase the interport isolation, four identical probes are applied here to link the top surface of the cavity and the ground plane for creating a new coupling path between the cavity and the patch antenna, as shown in Fig. 5. As we mentioned previously, the patch antenna and the cavity operate at TM_{01} and TE_{110} modes, respectively. The four probes have different influences on these two modes because their electric field distributions are dissimilar. The electric field distributions of the patch antenna and the CBSA with four probes added are shown in Fig. 6(a) and (b), respectively. The TE_{10} mode of the patch antenna is effectively excited, though the electric field distribution is uneven in the *XZ* plane due to the impact of the probes. As shown in Fig. 6(b), the TE_{110} mode of the CBSA is almost unchanged since the probes are placed where the electric field intensity of the TE_{110} mode is weak. The effect of probes would be further studied by parametric studies. Hence, near-field cancellation can be realized by combining the two out-of-phase coupling paths in theory.

Fig. 7 shows the S-parameters of the IBFD antenna with and without the CPC path. The results show that the MC level is reduced to < -25 dB within the common bandwidth and very high isolation value of 41.4 dB is obtained around 6.28 GHz when the CPC path is added. This phenomenon indicates that the four probes introduce another coupling path and effectively eliminate the SPC.

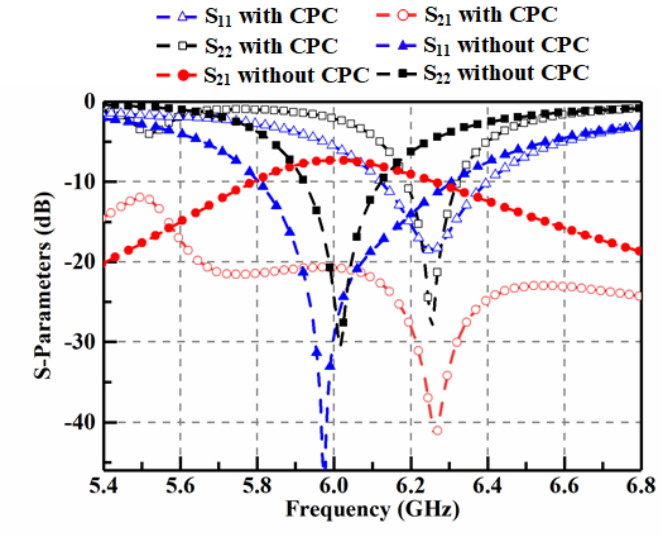

Fig. 7. Simulated S-parameters of the proposed antennas with/without the CPC path.

C. CPC Study

As shown in Fig. 2, relatively strong electric field intensity distributions are detected on the left and right edges of the patch antenna when the TM_{01} mode is excited. However, the electric field intensity of the TE_{110} mode is obviously weak on both sides. Thus, the four probes have totally different impacts on the operating frequencies of the patch antenna and the cavity.

The effect of the parameter l_3 on the S-parameters is shown in Fig. 8(a). The results show that both the resonant frequencies of the patch antenna and the interport isolation are affected by the parameter l_3, whose effect on the reflection coefficient of the CBSA is quite insignificant. As l_3 increases, the dip of MC moves to a lower frequency, whereas the resonant frequency of the Tx antenna shifts to a higher frequency. The influence of the parameter l_4 on the S-parameters was also investigated by varying it from 10.35 to 11.15 mm with 0.4 mm step in the range. As shown in Fig. 8(b), we found that the value l_4 does not have a significant impact on the operating frequency of the CBSA, while it obviously changes the working frequency of the patch antenna. This phenomenon is corresponding to the electric field distributions shown in Fig. 2. The peak electric field intensity on the patch antenna becomes stronger with an increase in l_4. Hence, the resonant frequency of the patch antenna varies obviously with different values of l_4. The four probes have little impact on the cavity mode due to the fact that the electric field distribution of the cavity is not affected seriously by the probes. It is noted that S_{21} is sensitive to the parameter l_4 because the coupling energy and phase are affected simultaneously by changing l_4.

As l_4 increases, the dip of MC and the operating frequency of the Tx antenna show reverse trends. This phenomenon can also be seen in Fig. 8(a). As the parameters l_3 and l_4 alter, both the coupling energy and phase of the two coupling paths vary due to the change of the resonant frequency of the patch antenna. As a result, the resonant frequency of the

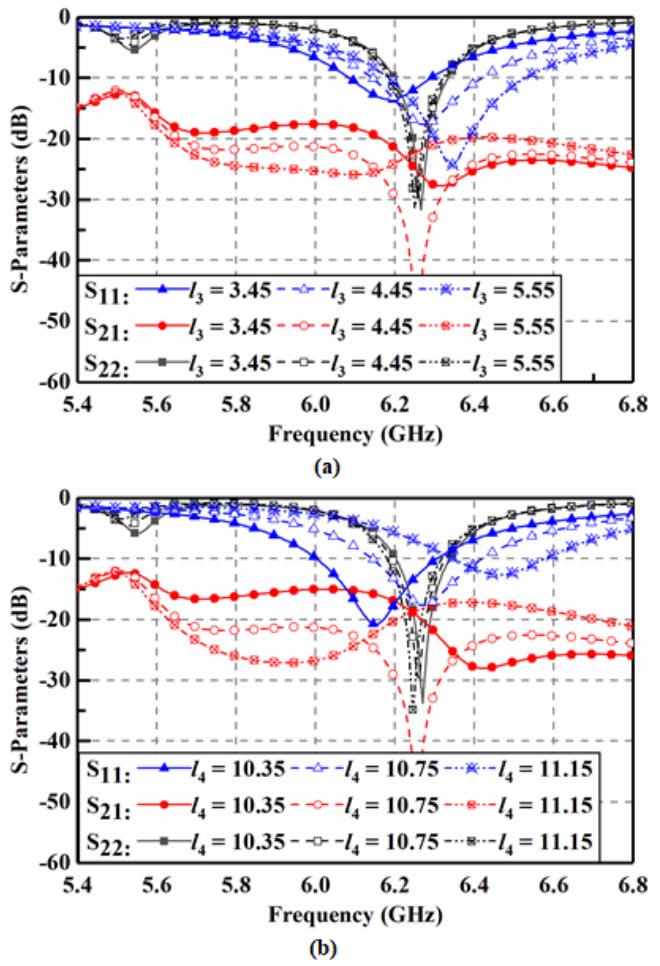

Fig. 8. Simulated S-parameters of the proposed antenna for different (c) l_3 and (d) l_4 (unit: mm).

patch antenna and the MC between the cavity and the patch can be tuned by changing parameters l_3 and l_4. As shown in Fig. 8(a) and (b), it is obvious that the resonant frequencies of the patch antenna and the CPC are more sensitive to the parameter l_4 than the parameter l_3 because the electric field distribution of the TM_{01} mode is almost uniform in the XZ plane.

D. SPC Study

Fig. 9 shows the variation of the S-parameters with respect to different slot lengths w_2. The increase of w_2 gives rise to a lower resonant frequency of the CBSA. It can be observed that the dip of the MC and the operating frequency of the CBSA show the same trends with the increase of w_2. Meanwhile, the return loss of the patch changes slightly. Hence, the SPC and the working frequency of the Rx antenna can be adjusted simultaneously with similar trends by adjusting parameter w_2.

E. Design Guidelines

Based on the analysis above, design guidelines are given as follows.

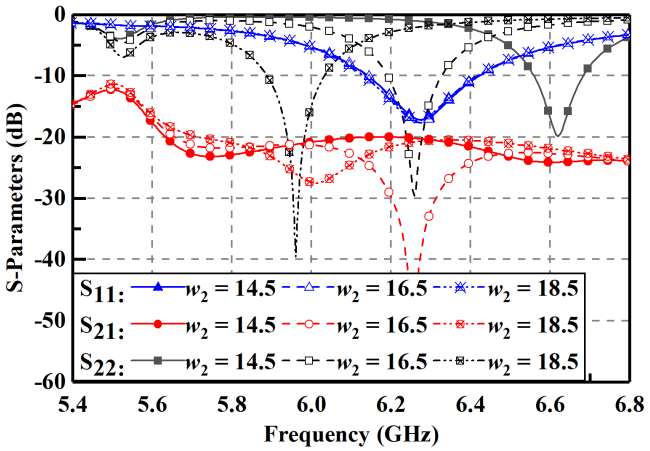

Fig. 9. Simulated S-parameters with different values of w_2 (unit: mm).

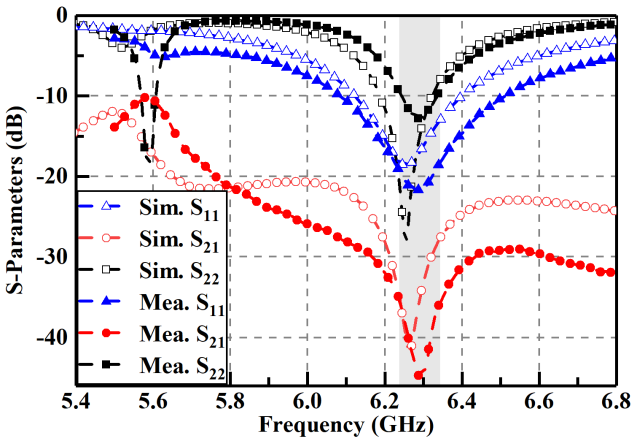

Fig. 11. Simulated and measured S-parameters of the proposed antenna.

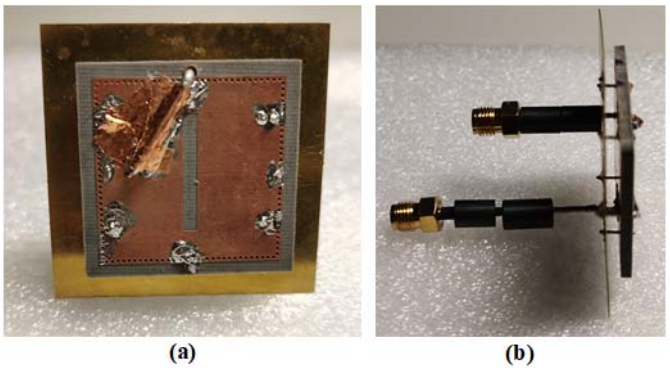

Fig. 10. Fabricated prototype of the proposed antenna. (a) Front view. (b) Side view.

1) Based on the target frequency (f_0), select the length (l_1) of the square patch as $0.5\lambda_0$ initially for exciting the TM_{01} mode. A substrate with proper dielectric constant is selected for reducing the resonant frequency of the CBSA (f_1, $f_1 < f_0$). The width of the square substrate is broader than that of the patch for easier fabrication and soldering. The resonant frequency of the patch antenna (f_2) moves to a lower frequency due to the effect of the larger substrate. It is noted that the operating frequency of the patch antenna (f_2) should be lower than f_1 in consideration of the probe's effect in the next step.

2) Four probes are added to realize field cancellation at frequency f_1 by carefully adjusting the values of l_3 and l_4, while the patch antenna resonates at frequency f_2 ($f_2 = f_0$). In other words, the dip of S_{21} can be moved to the resonant frequency (f_1) of the Rx antenna by varying l_3 and l_4.

3) The value of w_2 is tuned to shift the resonant frequency of the CBSA to the frequency f_2. Then, the values of l_3, l_4, and w_2 are fine-tuned to realize better performance.

IV. Experimental Verification

A. Antenna Fabrication

The designed co-LP stacked IBFD antenna was fabricated based on the optimized parameter values. Fig. 10 shows the fabricated prototype of the proposed antenna. The antenna is fed by 50 Ω coaxial cables. The mainboard was fabricated by printed circuit board process with a 2 mm-thick F4B substrate ($\varepsilon_r = 2.65$ and loss tangent of 0.0015). The metal ground was manufactured by a 0.3 mm-thick brass plate ($\sigma = 1.5 \times 10^7$ S/m) with a laser cutting process. As shown in Fig. 10(a), the metal walls are realized by the SIW technology. The size of the substrate is $30 \times 30 \times 2$ mm^3. A coaxial cable in the central plane of the patch antenna passes through the substrate, feeding the CBSA and serving as a support simultaneously. The performance of the patch antenna is unaffected by the coaxial cable since an equivalent electric wall is obtained in the central plane of the patch antenna, as shown in Fig. 2(a). The coaxial cable was bent so that it can be soldered to the top layer of the CBSA. Also, the inner conductor of the coaxial cable was soldered to the bottom layer of the CBSA for exciting the TE_{110} mode. Besides, magnetic beads were used to suppress the adverse effect of feeding RF cables when radiation patterns are measured.

B. S-Parameters

Fig. 11 shows the measured and simulated S-parameters. The measured S-parameters of the designed antenna were measured using an N5071B vector network analyzer (300 kHz–9 GHz) in an anechoic chamber. The measured −10 dB bandwidths of the Tx and Rx antennas are 6.08–6.51 and 6.24–6.34 GHz, respectively. Overlaying bandwidth of the IBFD antenna is 100 MHz. Both the simulated and measured results show that the MC level between the Tx and Rx antennas is less than −40 dB at the center frequency and less than −25 dB within the 10 dB impedance bandwidth. The measured S_{21} shows better performance than simulated S_{21} since the measured S_{22} deteriorates. It can be seen that slight resonant frequency shifting between the simulation and measurement occurs and the measured −10 dB bandwidth of the CBSA is narrower than the simulated one. The discrepancy between the measurement and simulation is mainly caused by the fabrication error, uneven ground plane, and machining accuracy. Two important parameters related to antenna performance were

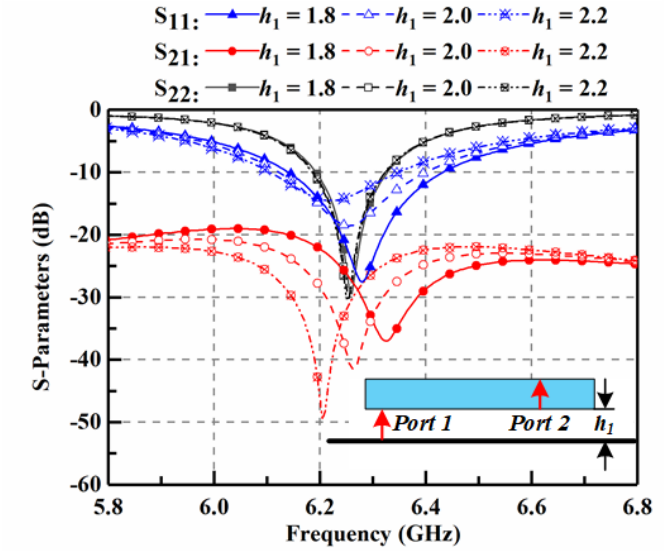

Fig. 12. S-parameters for different profiles of the patch antenna (unit: mm).

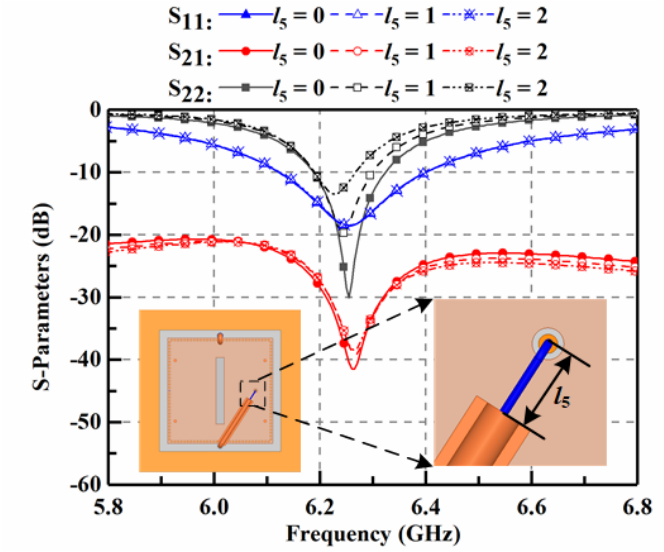

Fig. 13. S-parameters for different values of l_5 (unit: mm).

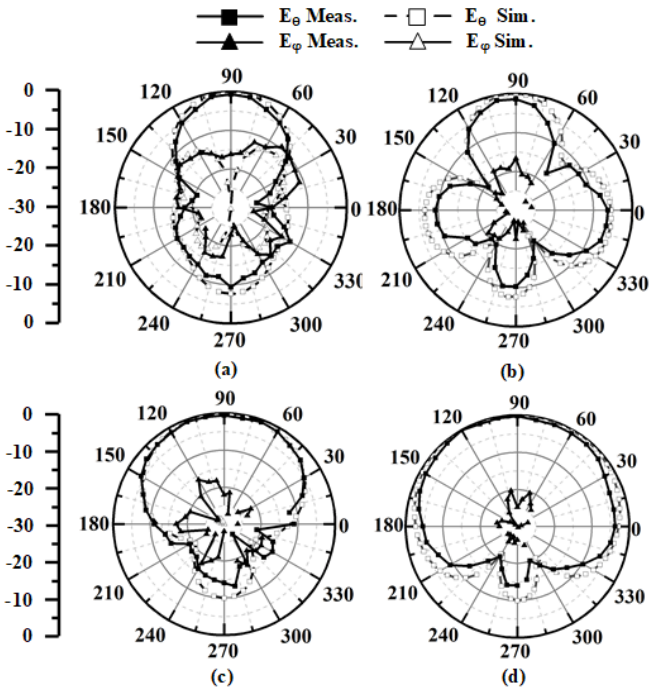

Fig. 14. Simulated and measured normalized radiation patterns of the proposed antenna at 6.28 GHz. (a) Port 1 in *XZ* plane. (b) Port 1 in *YZ* plane. (c) Port 2 in *XZ* plane. (c) Port 2 in *YZ* plane.

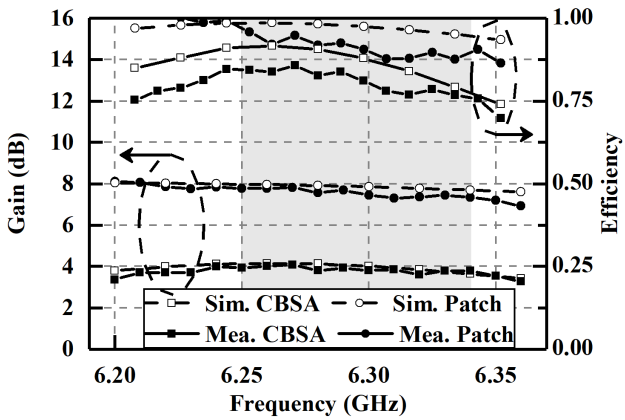

Fig. 15. Gain and efficiency of the proposed antenna.

studied, namely, the profile (h_1) of the patch antenna and the inner conductor length (l_5) of the coaxial line for port 2. The two parameters brought errors in the process of fabrication. Hence, two simulations with different values of h_1 and l_5 have been carried out. Fig. 12 shows the variation of S-parameters with different values of h_1. The changes of interport isolation and bandwidth of the patch antenna with variant h_1 show similar trends. The increase of parameter h_1 contributes to a rise of the highest isolation. The phenomenon demonstrates that the near-field cancellation is affected by the profile of the patch antenna. Another important parameter l_5 has an important impact on S_{22}, as presented in Fig. 13. S_{11} and S_{21} are almost unchanged with different values of l_5. However, according to the results from Fig. 13, the increase of parameter l_5 will decrease the operating bandwidth of the CBSA due to the parasitic effect of the coaxial line. Therefore, the inner conductor length of the coaxial line for port 2 should be as short as possible in the welding process.

C. Radiation Performance

In Fig. 14, the measured and simulated radiation patterns of the fabricated prototypes at 6.28 GHz are plotted with good agreement between simulation and measurement. For better demonstrating, the data have been normalized. The good broadside radiation patterns of the Rx and Tx antennas are achieved in the elevation plane. Therefore, a co-LP stacked IBFD antenna with broadside radiation patterns is realized.

The radiation characteristics of the fabricated prototype were also studied. The radiation gains and total efficiency are presented in Fig. 15 as functions of frequency. The gain

TABLE II
COMPARISON AMONG THE CO-POLARIZED IBFD ANTENNAS

Reference	Method	Size (λ_0^3)	BW (%)	No Feeding Networks	Integrated Structure	Polarization/ Pattern	Structure	Range of Isolation Levels (dB)
[17]	Spatial phase diversity	1.96 × 1.96 × 0.02	4.1	×	√	CP/ Broadside	Planar	41 - 54
[18]	Spatial phase diversity	1.51 × 1.51 × 0.47	98	×	√	LP/ Omnidirectional	3D	40 - 53
[19]	Spatial phase diversity	1.63 × 1.63 × 0.04	4.1	×	×	CP/ Broadside	3D	47 - 63
[20]	Spatial phase diversity	0.44 × 0.44 × 0.15	11.8	×	√	LP/ Omnidirectional	3D	40 - 63
[23]	Parasitic structure	1.65 × 0.63 × 0.01	12.2	√	√	LP/ Omnidirectional	Planar	50 - 75
[24]	Parasitic structure	2.94 × 1.52 × 0.01	11.7	√	√	LP/ Omnidirectional	Planar	50 - 55
Our Work	Two coupling paths	0.63 × 0.63 × 0.08	1.6	√	√	LP/ Broadside	Stacked	25 - 41

and radiation patterns were measured in a far-field anechoic chamber. It is seen that the measured results agree well with the simulated ones. The patch antenna and CBSA have average gains of 7.58 and 3.87 dB, respectively. It exhibits that the average efficiencies of the Tx and Rx antennas are 92% and 81%, respectively.

Table II shows the properties of the proposed antenna in comparison with the other presented IBFD antennas. Two co-circularly polarized antennas proposed in [17] and [19] have wider bandwidth and better interport isolation. Feeding networks used in these works take up a certain space. The proposed antenna with simple feed has a relatively small size. As shown in Fig. 3, the original isolation of the proposed IBFD antenna without the CPC patch is only 7 dB. Hence, it is reasonable that a narrow bandwidth is obtained as the isolation is improved. The proposed structure shows an acceptable compromise between the size, profile, and bandwidth. The proposed antenna can be used in many communication systems with narrow bandwidth, such as public safety and intelligent transportation systems.

V. CONCLUSION

In this work, a stacked co-LP IBFD antenna with broadside radiation patterns and compact size is proposed based on near-field cancellation. Both the simulation and test results show that the proposed IBFD antenna can provide isolation higher than 40 dB at the center frequency and more than 25 dB within the 10 dB impedance bandwidth. For both the Tx and Rx antennas, broadside performance is achieved in a compact size. The deigned antenna offers a new solution to the stacked co-LP broadside IBFD antenna with the advantages of relatively simple feed and compact size, having the potential for several applications, including public safety, intelligent transportation systems, and military communications.

REFERENCES

[1] J. I. Choi, M. Jain, K. Srinivasan, P. Levis, and S. Katti, "Achieving single channel, full duplex wireless communication," in *Proc. 16th Annu. Int. Conf. Mobile Comput. Netw. (MobiCom)*, 2010, pp. 1–12.

[2] V. Singh, A. Gadre, and S. Kumar, "Full duplex radios," in *Proc. 19th ACM Workshop Hot Topics Netw.*, Hong Kong, Nov. 2020, pp. 375–386.

[3] D. Korpi, M. Heino, C. Icheln, K. Haneda, and M. Valkama, "Compact inband full-duplex relays with beyond 100 dB self-interference suppression: Enabling techniques and field measurements," *IEEE Trans. Antennas Propag.*, vol. 65, no. 2, pp. 960–965, Feb. 2017.

[4] E. A. Etellisi, M. A. Elmansouri, and D. S. Filipovic, "In-band full-duplex multimode lens-loaded eight-arm spiral antenna," *IEEE Trans. Antennas Propag.*, vol. 66, no. 4, pp. 2084–2089, Apr. 2018.

[5] E. A. Etellisi, M. A. Elmansouri, and D. S. Filipovic, "Wideband monostatic simultaneous transmit and receive (STAR) antenna," *IEEE Trans. Antennas Propag.*, vol. 64, no. 1, pp. 6–15, Jan. 2016.

[6] M. A. Elmansouri, A. J. Kee, and D. S. Filipovic, "Wideband antenna array for simultaneous transmit and receive (STAR) applications," *IEEE Antennas Wireless Propag. Lett.*, vol. 16, pp. 1277–1280, 2017.

[7] H. Nawaz and I. Tekin, "Dual-polarized, differential fed microstrip patch antennas with very high interport isolation for full-duplex communication," *IEEE Trans. Antennas Propag.*, vol. 65, no. 12, pp. 7355–7360, Dec. 2017.

[8] I. Acimovic, D. A. McNamara, and A. Petosa, "Dual-polarized microstrip patch planar array antennas with improved port-to-port isolation," *IEEE Trans. Antennas Propag.*, vol. 56, no. 11, pp. 3433–3439, Nov. 2008.

[9] Y. Su and Z. N. Chen, "Isolation improvement and beam manipulation of dual-polarized RIS-halved lens antennas for compact transceiver systems," *IEEE Trans. Antennas Propag.*, vol. 67, no. 9, pp. 5877–5884, Sep. 2019.

[10] M. R. Nikkhah, J. Wu, H. Luyen, and N. Behdad, "A concurrently dual-polarized, simultaneous transmit and receive (STAR) antenna," *IEEE Trans. Antennas Propag.*, vol. 68, no. 8, pp. 5935–5944, Aug. 2020.

[11] D. Wojcik, M. Surma, A. Noga, and M. Magnuski, "High port-to-port isolation dual-polarized antenna array dedicated for full-duplex base stations," *IEEE Antennas Wireless Propag. Lett.*, vol. 19, no. 7, pp. 1098–1102, Jul. 2020.

[12] K. Wei and B.-C. Zhu, "The novel W parasitic strip for the circularly polarized microstrip antennas design and the mutual coupling reduction between them," *IEEE Trans. Antennas Propag.*, vol. 67, no. 2, pp. 804–813, Feb. 2019.

[13] H. Nawaz and I. Tekin, "Double-Differential-fed, dual-polarized patch antenna with 90 dB interport RF isolation for a 2.4 GHz in-band full-duplex transceiver," *IEEE Antennas Wireless Propag. Lett.*, vol. 17, no. 2, pp. 287–290, Feb. 2018.

[14] P. V. Prasannakumar, M. A. Elmansouri, and D. S. Filipovic, "Wideband decoupling techniques for dual-polarized bi-static simultaneous transmit and receive antenna subsystem," *IEEE Trans. Antennas Propag.*, vol. 65, no. 10, pp. 4991–5001, Oct. 2017.

[15] E. Tsakalaki, E. Foroozanfard, E. de Carvalho, and G. F. Pedersen, "A 2-order MIMO full-duplex antenna system," in *Proc. 8th Eur. Conf. Antennas Propag. (EuCAP)*, Apr. 2014, pp. 2546–2550.

[16] L. Sun, Y. Li, Z. Zhang, and Z. Feng, "Compact co-horizontally polarized full-duplex antenna with omnidirectional patterns," *IEEE Antennas Wireless Propag. Lett.*, vol. 18, no. 6, pp. 1154–1158, Jun. 2019.

[17] Z. Zhou, Y. Li, J. Hu, Y. He, Z. Zhang, and P.-Y. Chen, "Monostatic copolarized simultaneous transmit and receive (STAR) antenna by integrated single-layer design," *IEEE Antennas Wireless Propag. Lett.*, vol. 18, no. 3, pp. 472–476, Mar. 2019.
[18] R. Lian, T.-Y. Shih, Y. Yin, and N. Behdad, "A high-isolation, ultra-wideband simultaneous transmit and receive antenna with monopole-like radiation characteristics," *IEEE Trans. Antennas Propag.*, vol. 66, no. 2, pp. 1002–1007, Feb. 2018.
[19] J. Ha, M. A. Elmansouri, P. Valale Prasannakumar, and D. S. Filipovic, "Monostatic co-polarized full-duplex antenna with left-or right-hand circular polarization," *IEEE Trans. Antennas Propag.*, vol. 65, no. 10, pp. 5103–5111, Oct. 2017.
[20] D. Wu, Y. Zang, H. Luyen, M. Li, and N. Behdad, "A compact, low-profile simultaneous transmit and receive antenna with monopole-like radiation characteristics," *IEEE Antennas Wireless Propag. Lett.*, vol. 18, no. 4, pp. 611–615, Apr. 2019.
[21] A. Diallo, C. Luxey, P. Le Thuc, R. Staraj, and G. Kossiavas, "Study and reduction of the mutual coupling between two mobile phone PIFAs operating in the DCS1800 and UMTS bands," *IEEE Trans. Antennas Propag.*, vol. 54, no. 11, pp. 3063–3074, Nov. 2006.
[22] A. Batgerel and S. Y. Eom, "High-isolation microstrip patch array antenna for single channel full duplex communications," *IET Microw., Antennas Propag.*, vol. 9, no. 11, pp. 1113–1119, Aug. 2015.
[23] K. Iwamoto, M. Heino, K. Haneda, and H. Morikawa, "Design of an antenna decoupling structure for an inband full-duplex collinear dipole array," *IEEE Trans. Antennas Propag.*, vol. 66, no. 7, pp. 3763–3768, Jul. 2018.
[24] J.-H. Xun, L.-F. Shi, W.-R. Liu, and D.-J. Xin, "A self-interference suppression structure for collinear dipoles," *IEEE Antennas Wireless Propag. Lett.*, vol. 18, no. 10, pp. 2100–2104, Oct. 2019.
[25] S. Zhang, S. N. Khan, and S. He, "Reducing mutual coupling for an extremely closely-packed tunable dual-element PIFA array through a resonant slot antenna formed in-between," *IEEE Trans. Antennas Propag.*, vol. 58, no. 8, pp. 2771–2776, Aug. 2010.
[26] M. A. Abdalla and A. M. Abdelraheem, "Compact transmit receive hybrid electromagnetic isolation in antenna array transceiver system for full duplex applications," *IET Microw., Antennas Propag.*, vol. 11, no. 3, pp. 417–425, Feb. 2017.
[27] S. N. Venkatasubramanian, L. Li, A. Lehtovuori, C. Icheln, and K. Haneda, "Impact of using resistive elements for wideband isolation improvement," *IEEE Trans. Antennas Propag.*, vol. 65, no. 1, pp. 52–62, Jan. 2017.
[28] S. Manafi, M. A. Al-Tarifi, and D. S. Filipovic, "Isolation improvement techniques for wideband millimeter-wave repeaters," *IEEE Antennas Wireless Propag. Lett.*, vol. 17, no. 2, pp. 355–358, Feb. 2018.
[29] S. Long and M. Walton, "A dual-frequency stacked circular-disc antenna," *IEEE Trans. Antennas Propag.*, vol. 27, no. 2, pp. 270–273, Mar. 1979.
[30] R. Q. Lee, K. F. Lee, and J. Bobinchak, "Characteristics of a two layer electromagnetically coupled rectangular patch antenna," *Electron. Lett.*, vol. 23, pp. 1070–1072, Sep. 1987.
[31] E. Rajo-Iglesias, G. Villaseca-Sánchez, and C. Martín-Pascual, "Input impedance behavior in offset stacked patches," *IEEE Antennas Wireless Propag. Lett.*, vol. 1, pp. 28–30, Jan. 2002.
[32] Ó. Quevedo-Teruel, Z. Sipus, and E. Rajo-Iglesias, "Characterization and reduction of mutual coupling between stacked patches," *IEEE Trans. Antennas Propag.*, vol. 59, no. 3, pp. 1031–1036, Mar. 2011.

Weiquan Zhang received the B.S. degree from the University of Electronic Science and Technology of China, Chengdu, China, in 2018. He is currently pursuing the Ph.D. degree in electrical engineering with Tsinghua University, Beijing, China.

His current research interests include reconfigurable antennas, multimode antennas, and reflectarray antennas.

Jiadong Hu received the B.S. degree from Xidian University, Xi'an, China, in 2017. He is currently pursuing the Ph.D. degree in electrical engineering with Tsinghua University, Beijing, China.

His current research interests include antenna decoupling, reconfigurable antennas, and beam scanning array.

Yue Li (Senior Member, IEEE) received the B.S. degree in telecommunication engineering from Zhejiang University, Hangzhou, Zhejiang, China, in 2007, and the Ph.D. degree in electronic engineering from Tsinghua University, Beijing, China, in 2012.

In June 2012, he was a Post-Doctoral Fellow with the Department of Electronic Engineering, Tsinghua University. In December 2013, he was a Research Scholar with the Department of Electrical and Systems Engineering, University of Pennsylvania, Philadelphia, PA, USA. He was a Visiting Scholar with the Institute for Infocomm Research (I2R), A∗STAR, Singapore, in 2010, and the Hawaii Center of Advanced Communication (HCAC), University of Hawaii at Mānoa, Honolulu, HI, USA, in 2012. Since January 2016, he has been with Tsinghua University, where he is also an Assistant Professor. He is currently an Associate Professor with the Department of Electronic Engineering, Tsinghua University. He has authored or coauthored over 150 journal articles and 45 international conference papers. He holds 20 granted Chinese patents. His current research interests include metamaterials, plasmonics, electromagnetics, nanocircuits, mobile and handset antennas, multiple-input–multiple-output (MIMO) and diversity antennas, and millimeter-wave antennas and arrays.

Dr. Li was a recipient of the Issac Koga Gold Medal from the URSI General Assembly in 2017; the Second Prize of Science and Technology Award of China Institute of Communications in 2017; the Young Scientist Awards from the conferences of PIERS 2019, ACES 2018, AT-RASC 2018, AP-RASC 2016, EMTS 2016, and URSI GASS 2014; the Best Paper Awards from the conferences of APCAP 2020/2017, UCMMT 2020, ISAP 2019, CSQRWC 2018, NCMMW 2018/2017, NCANT 2019/2017, ISAPE 2016, and ICMMT 2020/2016; the Outstanding Doctoral Dissertation of Beijing Municipality in 2013; and the Principal Scholarship of Tsinghua University in 2011. He is serving as an Associate Editor for IEEE TRANSACTIONS ON ANTENNAS AND PROPAGATION, IEEE ANTENNAS AND WIRELESS PROPAGATION LETTERS, *Microwave and Optical Technology Letters*, and *Computer Applications in Engineering Education*. He serves on the Editorial Board of *Scientific Reports*.

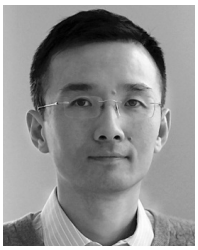

Zhijun Zhang (Fellow, IEEE) received the B.S. and M.S. degrees from the University of Electronic Science and Technology of China, Chengdu, China, in 1992 and 1995, respectively, and the Ph.D. degree from Tsinghua University, Beijing, China, in 1999.

In 1999, he was a Post-Doctoral Fellow with the Department of Electrical Engineering, The University of Utah, Salt Lake City, UT, USA, where he was appointed a Research Assistant Professor in 2001. In May 2002, he was an Assistant Researcher with the University of Hawaii at Mānoa, Honolulu, HI, USA. In November 2002, he joined Amphenol T&M Antennas, Vernon Hills, IL, USA, as a Senior Staff Antenna Development Engineer and was then promoted to the position of Antenna Engineer Manager. In 2004, he joined Nokia Inc., San Diego, CA, USA, as a Senior Antenna Design Engineer. In 2006, he joined Apple Inc., Cupertino, CA, USA, as a Senior Antenna Design Engineer and was then promoted to the position of Principal Antenna Engineer. Since August 2007, he has been with Tsinghua University, where he is currently a Professor with the Department of Electronic Engineering. He is the author of *Antenna Design for Mobile Devices* (Wiley, First Edition, 2011, and Second Edition, 2017).

Dr. Zhang served as an Associate Editor for the IEEE TRANSACTIONS ON ANTENNAS AND PROPAGATION from 2010 to 2014 and the IEEE ANTENNAS AND WIRELESS PROPAGATION LETTERS from 2009 to 2015.